Discover Chemistry

RESEARCH Open Access

Green-route synthesis of coordination polymers using terephthalic acid from plastic wastes for the removal of endocrine-disrupting chemical (Atrazine) from aqueous solution

Adedibu C. Tella[1,4*], Uchenna V. Ugwuanyi[1,8], Victoria T. Olayemi[2], Olalere G. Adeyemi[3], Hadley S. Clayton[4], Dele P. Fapojuwo[5], Margaret D. Olawale[6], Vincent O. Adimula[7*] and Samson O. Owalude[1]

*Correspondence:
Adedibu C. Tella
ac_tella@yahoo.co.uk
Vincent O. Adimula
adimula.vo@unilorin.edu.ng

Full list of author information is available at the end of the article

Abstract

Terephthalic acid (TPA) was successfully extracted from polyethylene terephthalate (PET) plastic bottles through alkaline hydrolysis. Coordination Polymers ($[Zn(TPA)_2(H_2O)_2]$, and $[Co(TPA)_2(H_2O)_2]$), and $[Ni(TPA)_2(H_2O)_2]$ (TPA = Terepthalic acid) were synthesized by grinding terepthalic acid extracted from the plastic waste with metal acetate salt via green synthetic method (ball-milling). These were characterised using FTIR, PXRD, BET, Melting Point analysis, UV–Vis spectroscopy, XRF and SEM techniques to investigate the functional groups, structural crystallinity, surface area, thermal stability, electronic transition, elemental composition and morphology of the material, respectively. Adsorption studies for the removal of endocrine-disrupting chemicals (Atrazine) were carried out to understand their applicability in the removal of pesticide residues from a polluted environment. The study also shows that the synthesized coordination polymers were favorable for Atrazine removal, for which $[Co(TPA)_2(H_2O)_2]$, $[Ni(TPA)_2(H_2O)_2]$, and $[Zn(TPA)_2(H_2O)_2]$ showed a maximum adsorption capacity of 41.322, 52.91 and 60.241 mg/g, respectively. The kinetics study shows that Atrazine adsorption followed a pseudo-first-order kinetics model. The thermodynamic parameters were calculated, and the results showed that the adsorption of Atrazine on the coordination polymers is a spontaneous and exothermic process. Therefore, all the synthesised coordination polymers are promising adsorbents for the removal of Atrazine pesticide in a polluted environment.

Keywords Adsorption, Synthesis, Coordination polymer, Terephthalic acid, Atrazine

1 Introduction

Pesticides are chemicals that can be used to facilitate the growth of plants, to prevent agricultural harvests from a variety of damages and to increase the production and yield of crops. The rapid and indiscriminate use of pesticides in modern agricultural practices for social benefits, such as to reduce crop losses, enhance yield and meet rising food

© The Author(s) 2025. **Open Access** This article is licensed under a Creative Commons Attribution-NonCommercial-NoDerivatives 4.0 International License, which permits any non-commercial use, sharing, distribution and reproduction in any medium or format, as long as you give appropriate credit to the original author(s) and the source, provide a link to the Creative Commons licence, and indicate if you modified the licensed material. You do not have permission under this licence to share adapted material derived from this article or parts of it. The images or other third party material in this article are included in the article's Creative Commons licence, unless indicated otherwise in a credit line to the material. If material is not included in the article's Creative Commons licence and your intended use is not permitted by statutory regulation or exceeds the permitted use, you will need to obtain permission directly from the copyright holder. To view a copy of this licence, visit http://creativecommons.org/licenses/by-nc-nd/4.0/.

needs, has become a matter of social accountability [7]. On the other hand, extensive consumption of a variety of pesticides has raised concerns at local, regional, national and global scales due to the fact that pesticide residues may be ingested by humans via food, drinking water and air, and are being bio-accumulated in blood, mother's milk, and tissues. Hence, pesticides contribute to symptomatic illnesses, both acute and chronic [12]. Over the last five years, pesticide imports into Africa have increased significantly [33].

Based on their application methods, between 10 and 75% of the pesticides do not reach their targets, resulting in frequent contamination of terrestrial and aquatic environments. The EU drinking water directive sets the general drinking water quality standard for added concentrations of pesticides and their metabolites to be less than 0.5 $\mu g \cdot L^{-1}$ [19]. Adsorption method using porous materials is considered an effective method to reduce the potential risks of various emerging pesticide contaminants in the environment, among which coordination polymers may be a group of promising porous materials due to their porous nature and the versatility in building blocks and functionality [28]. Coordination polymers have gotten attention as a new kind of adsorbent and have been applied for the adsorption of Pesticides [42].

Coordination polymers are crystalline compounds consisting of metal clusters coordinated to organic ligands to form one-, two-, or three-dimensional porous structures (Yaghi et al., 2003). CPs have high surface area, high pore volume, and low framework density [10]. CPs are a class of coordinate polymers consisting of 2D and 3D network topologies formed from the combination of metal ions and organic linkers [39]. They have simple and easy synthesis methods, favouring their adsorption performances and regeneration abilities with huge surface areas and accessible, tunable pores at comparatively low temperatures [14, 27]. The structures of CPs consist of metal ions and organic ligands linked together via coordination bonds. They possess permanent porosity and have unique properties such as large surface areas (1000–10,400 m^2/g), high thermal stability with tunable polarity and nanoscale pore sizes [35]. Our group previously reported the green route synthesis of coordination polymers (CPs) for environmental remediation [5, 38]. In continuation of our studies on the use of green route mechanochemical synthesis for the preparation of Coordination polymers for environmental remediation, herein, we report the synthesis of $[Co(TPA)_2(H_2O)_2]$, $[Ni(TPA)_2(H_2O)_2]$ and $[Zn(TPA)_2(H_2O)_2]$ using terepthalic acid extracted from plastic waste and comparison of their application as an adsorbent for removal of Atrazine pesticide from water. To the best of our knowledge, these coordination polymers have not been applied as an adsorbent for the uptake of any endocrine-disrupting chemical (such as Atrazine) from water.

2 Experimental

2.1 Materials and methods

2.1.1 Chemicals and reagents

All chemicals and reagents used in this study were analytical grade. This includes; Sodium hydroxide (NaOH, 98%, BDH, England), Hydrochloric acid (HCl, 37%, BDH, England), Zinc acetate (98% Loba Chemie, India), Nickel acetate (98% Loba Chemie, India), Cobalt acetate (98% BDH, England), Atrazine (80%, Blulux, India), Methanol (99.9%, Loba Chemie, India), Benzene-1,4-dicarboxylic (BDC)/Terephthalic acid (98%, Sigma Aldrich, Germany), and deionized water.

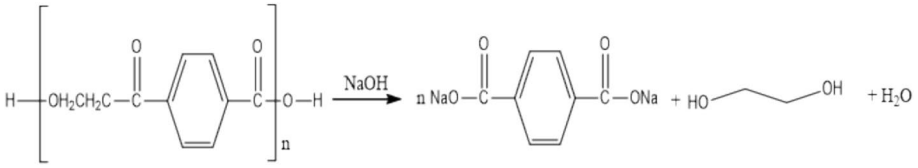


Fig. 1 Depolymerisation reaction of PET

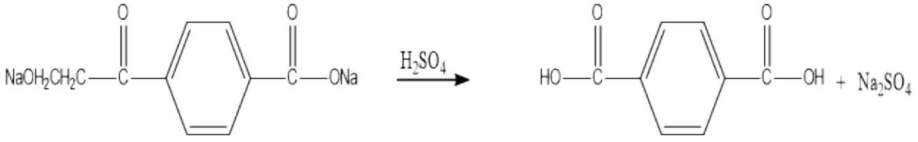


Fig. 2 Neutralisation reaction of disodium terephthalate

2.1.2 Extraction of terephthalic acid (TPA) from plastic wastes

The PET decomposition reaction was conducted in a 5 L stainless-steel autoclave reaction vessel suitable for temperatures above 100°C. The reactor was equipped with a digital temperature control system, an agitator, and a manometer as a pressure indicator.

Pellets of sodium hydroxide (22.5 g, 0.5625 mol) were dissolved in 500 mL of distilled water, and the resultant NaOH solution (1.125 M) was fed into the reactor. PET flakes (50 g, 0.26 mol) were then added and agitated. The temperature controller was set to the desired point, and when the desired temperature was reached, the PET decomposition process began for a specified time period [6]. After that period, the reactor was cooled with cold water for 5 min. The reaction mixture was neutralised to pH 6.5 with HCl and filtered to remove the unreacted PET solids. The TPA in the mixture was precipitated by acidification with HCl to a pH of 2.5. Finally, the mixture was filtered and washed with methanol. The solid TPA produced was dried, washed with methanol, filtered with a vacuum pump and dried in an oven at 80°C for 2 to 3 days and weighed. [25]. The equations of reaction are shown in Figs. 1 and 2.

3 Synthesis of coordination polymers using mechanochemical methods

$[Ni(TPA)_2(H_2O)_2]$ was synthesized by ball milling of 1:2 (molar ratio) mixtures of 20.0 mmol (3.3226 g) of benzene 1, 4-dicarboxylic acid and 10.0 mmol (2.4884 g) $Ni(OAc)_2{\cdot}4H_2O$ [31], also $[Zn(TPA)_2(H_2O)_2]$ was synthesized by ball milling of 1:2 (molar ratio) mixtures of 20.0 mmol (3.3226 g) of benzene 1, 4-dicarboxylic acid and 10.0 mmol of zinc(II) acetate dihydrate (2.195 g), The $[Co(TPA)_2(H_2O)_2]$ was synthesized by ball milling of 1:2 (molar ratio) mixtures of 20.0 mmol (3.3226 g) of benzene 1, 4-dicarboxylic acid and 10.0 mmol of colbalt acetate (2.4884 g), mixed using a mortal and pestle, homogenized for about 20 min and introduced into the ball milling machine to blend the mixture properly for about 30 min. De-ionised water (1 ml) was added, thereafter, to facilitate the reaction. The CP was activated in an oven at 80 °C for several hours (8 h). The enlarged scale reaction was performed with three or five times the benzene 1,4-dicarboxylic acid and metal precursor mixture [38].

$$M(CH_3COO)_2 + TPA + H_2O \underset{\text{Ball - milling}}{\overset{\text{Grindiing}}{\longrightarrow}} [N_i\,(TPA)_2\,(H_2O)_2]\,CH_3COOH$$

Activation was done mainly to remove or take out the trapped solvent, like water, acetic acid, methanol, etc., in the synthesised complex [37].

4 Adsorption studies

An exact amount (0.01 g) of the coordination polymer adsorbent was placed in the aqueous solution (10 ml) of Atrazine concentration from 20 to 100 ppm. The aqueous Atrazine solution containing the coordination polymer adsorbent was mixed with a mechanical shaker at 150 rpm for a fixed time of 2 h at room temperature. After adsorption at a pre-determined time, the solutions were separated from the adsorbent using a centrifuge, and the supernatant concentration after adsorption was calculated using the absorbance obtained from the UV–visible spectrophotometer at the pre-determined λ max wavelength of Atrazine. The amount of Altrazine absorbed per gram of the CP adsorbent(qe) was then calculated using the equation below [37].

$$Qe = \frac{v\,(Co - Ce)}{w} \tag{1}$$

C_0 = initial concentration of Atrazine mg/g, C_e = final concentration of the Atrazine mg/g, V = volume of the Atrazine (L) and w = weight of the CP.

5 Results and discussion

5.1 FT-IR spectra analysis of the extracted terephthalic acid

The FTIR spectrum (Fig. 3) of the synthesized terephthalic acid was collected to confirm that the synthesised terephthalic acid ligand matches that of the standard by comparing the functional groups on the surface of both materials. The broad peaks around 3419 cm^{-1} in both spectra could be assigned to the OH groups at the surface of both compounds. The carboxylate group of both exhibited two strongly coupled C – O bonds, which give rise to two sharp peaks, a symmetric C – O stretching band at 1398 cm^{-1} and an asymmetric C – O stretching band at 1586 cm^{-1}. In addition to the peak existing at 1586 cm^{-1}, the small bands at 1504 cm^{-1} could be assigned to the C = C of the benzene ring in the structure of both samples. The peak near 800 cm^{-1} shows a para-substituted

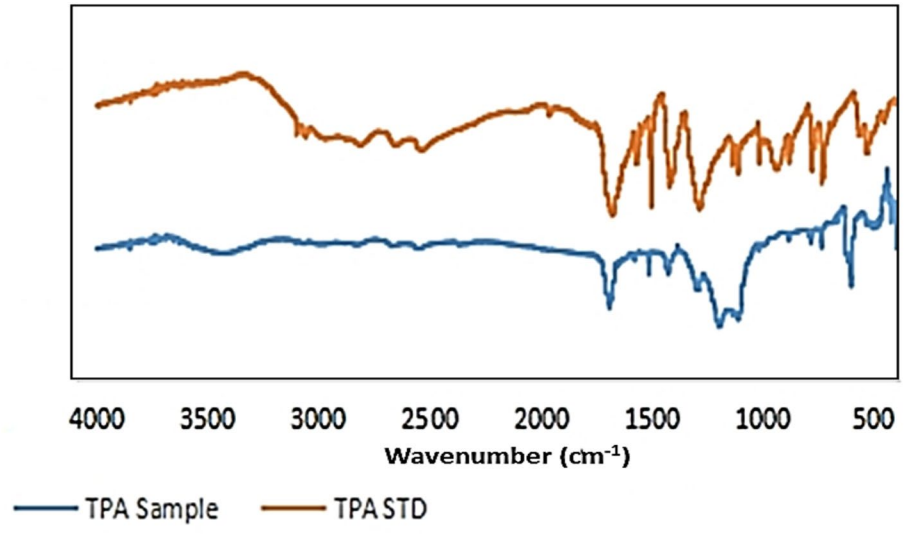


Fig. 3 FTIR results showing synthesized TPA and its Standard

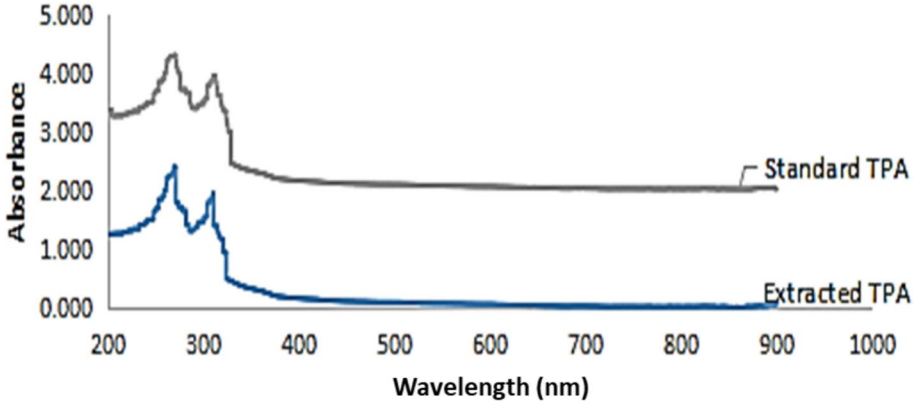


Fig. 4 UV–Vis spectra showing extracted TPA and its standard

Table 1 UV–visible spectra results of synthesised TPA and its standard

TPA Standard	Wavelength (nm)	Transition
	266	$\pi \rightarrow \pi^*$
	315	$n \rightarrow \pi^*$
TPA Sample	272	$\pi \rightarrow \pi^*$
	310	$n \rightarrow \pi^*$

Table 2 Physical properties of extracted TPA and standard TPA

Properties	Extracted TPA	Standard TPA
Melting point (°C)	302	300
pH	3.94	3.85

benzene, which is present in both samples. The FTIR spectra of both samples were therefore matched, and the two compounds were essentially the same. The results are in agreement with the findings of reported work on the synthesis of terephthalic acid by Karayannidis et al. [25].

5.2 UV–visible spectra analysis of extracted TPA and standard TPA

The sample was prepared by dissolving 0.32 g of TPA in a 4 mL aqueous solution of 2N potassium hydroxide. The absorbance of the solution was measured on a UV–visible spectrophotometer (Perkin Elmer Lambda Bio 20) from 200 to 900 nm using water as a control in a 1.0 cm cell.

From the UV–visible spectra (Fig. 4) and Table 1 results shown above, there was a strong absorption at the UV region of 266 nm for the TPA standard and 272 nm for the TPA sample, which signifies the presence of a ($\pi \rightarrow \pi^*$). The strong absorption at the UV region around 315 nm for the TPA standard and 310 nm for the extracted TPA sample indicates the ($n \rightarrow \pi*$) transition in both samples. In all cases, the spectra of the extracted TPA and the standard are almost identical, suggesting that they are the same materials [8].

Comparison of the solubility, pH and melting points of the two samples shows no distinct difference in their values as shown in Tables 2 and 3. It can be observed that extracted TPA and standard TPA are insoluble in ethanol and water. They are, to some extent, soluble in DMSO. The Melting point is, however, within the range of that reported for terephthalic acid.

Table 3 Solubility of the Extracted TPA and Standard TPA

Solvent	Sample Code	% Solubility
Ethanol	Extracted TPA	0.26
	Standard TPA	0.23
Water	Extracted TPA	0.01
	Standard TPA	0.01
DMSO	Extracted TPA	17.83
	Standard TPA	16.77

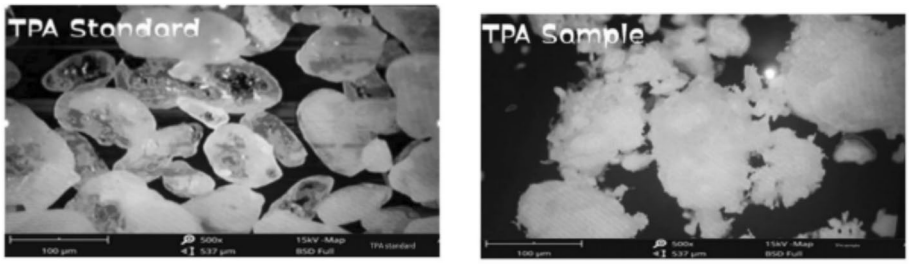


Fig. 5 SEM image of standard TPA and extracted TPA

5.3 SEM analysis results

The surface morphologies and chemical compositions of the extracted TPA (Fig. 5a) and the standard TPA (Fig. 5b) were studied by scanning electron microscopy (SEM) as presented below. At 500 × magnification, the image of the standard TPA showed a block microcrystalline when compared to the extracted TPA, which showed irregular aggregates with a smaller particle size [13].

5.4 PXRD analysis of the extracted TPA

The PXRD patterns of the extracted TPA are presented in Fig. 6. The pattern of the PXRD shows major peaks at 2θ values of 27.84°, this was followed by 17.26°, then by 25.04°, and lastly 40.50°. The results compare favourably with the work reported by Kaduk JA [24] and also when these data were compared to the Cambridge Crystallographic Data Centre (CCDC), the powder diffraction pattern of the sample is identical to that of standard TPA, with CCDC no. 718666, previously reported by [22].

5.5 FT-IR spectra analysis of synthesised coordination polymers

It can be deduced from Table 4 and Fig. 7 that the extracted CPs have a spectrum different from that of the ligand. For the absorption bands of the ligand for the $[Ni(TPA)_2(H_2O)_2]$, the ν_s (O–H) of the ligand was seen at 3429 cm^{-1}, while the ν_{as} (O–H) was observed between 2962 and 2827 cm^{-1}. This was shifted to ν_s (O–H) 3610 cm^{-1} and ν_s (O–H) between 2999 and 3066 cm^{-1}, in the CP. There is also a shift in ν_{as} (C = O) of the ligand from 1685 cm^{-1} to ν_{as} (C = O) around 1665 cm^{-1} but the ν_{as} (C = C) was observed at 1581 cm^{-1} in the CP, and a ν_s (M–O) band was seen around 416 cm^{-1} which suggests a coordination of the ligand to the metal, confirming the formation of new product which is $[Ni(TPA)_2(H_2O)_2]$.

(NB: Zn-MOF = $[Zn(TPA)_2(H_2O)_2]$, Co-MOF = $[Co(TPA)_2(H_2O)_2]$, and Ni-MOF = $[Ni(TPA)_2(H_2O)_2]$).

For $[Zn(TPA)_2(H_2O)_2]$, the ν_s (O–H) of the ligand was observed at 3429 cm^{-1}, while the ν_{as} (O–H) was seen between 2962–2827 cm^{-1}. This was reduced to ν_s (O–H) at

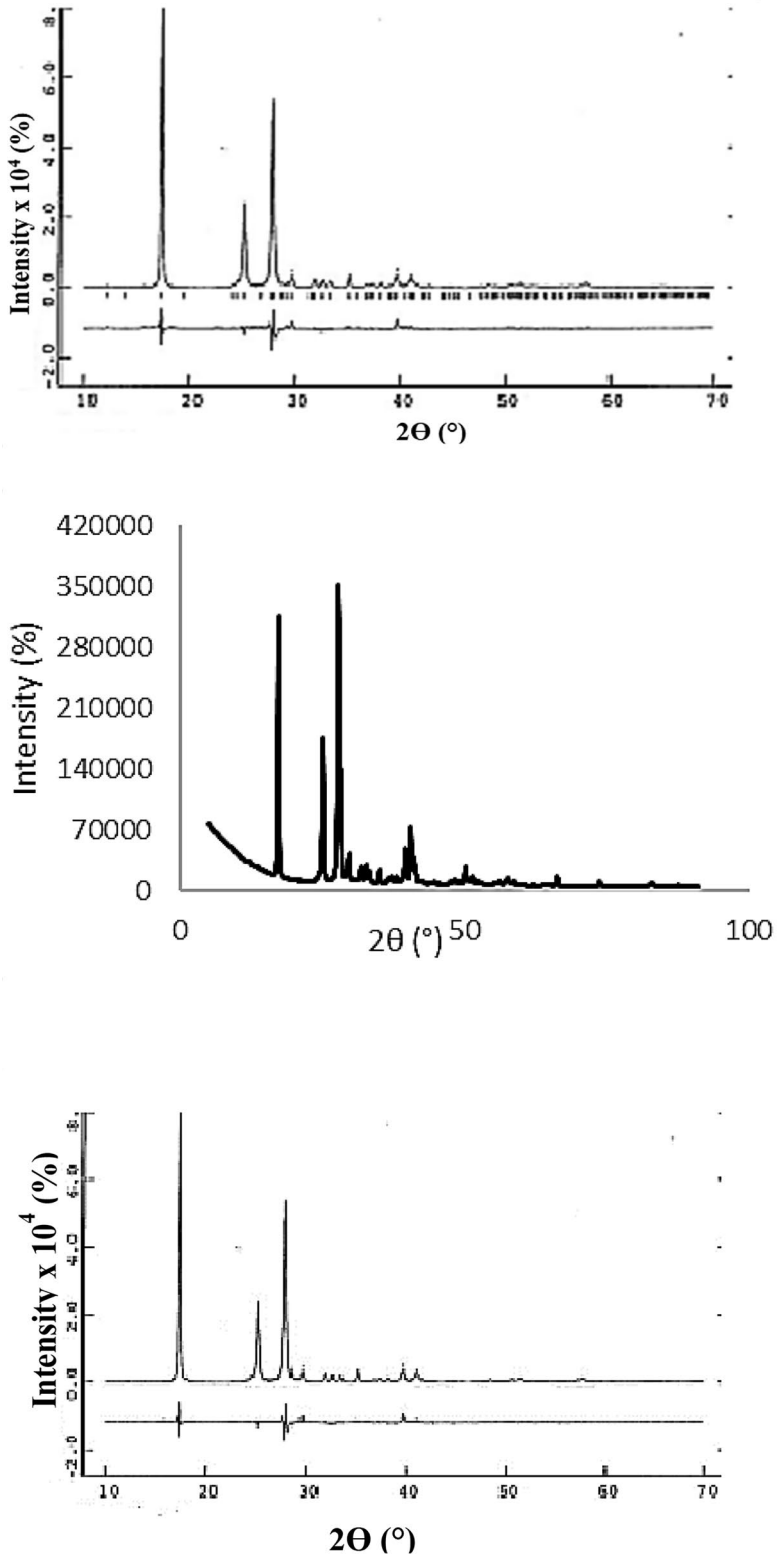


Fig. 6 PXRD pattern of extracted TPA and reported work

Table 4 Results of FT-IR spectra of each of the CPs

Ligand/CPs	ν(OH) cm^{-1}	ν(C = O) cm^{-1}	ν(C = C) cm^{-1}	ν(C-O) cm^{-1}	ν(M–O) cm^{-1}
Extracted TPA	3429	1685	1573	1192	–
$[Ni(TPA)_2(H_2O)_2]$	3610	1665	1581	1292	416
$[Zn(TPA)_2(H_2O)_2]$	3163	1685	1558	1388	594
$[Co(TPA)_2(H_2O)_2]$	3421	1665	1558	1284	443

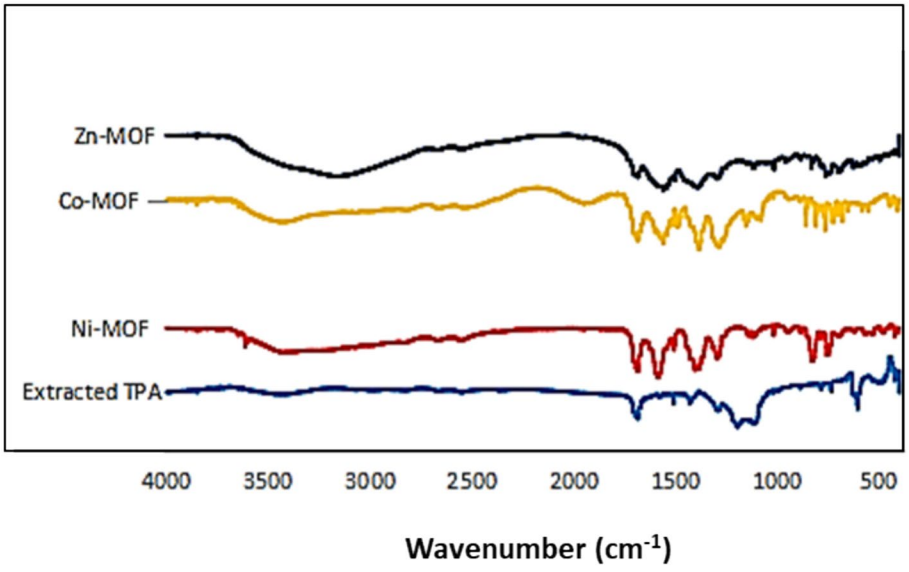


Fig. 7 Result showing FT-IR of each of the CPs

3163 cm^{-1} in the CP. There is no shift in ν_{as} (C = O) of the ligand and that of the CP as they maintain absorption at 1685 cm^{-1}, and the ν_s (M–O) band was seen around 594 cm^{-1}, which suggests the coordination of the ligand to the metal, confirming the formation of a new product $[Zn(TPA)_2(H_2O)_2]$.

For $[Co(TPA)_2(H_2O)_2]$, the ν_s (O–H) of the ligand are at 3429 cm^{-1}, and the ν_{as} (O–H) are between 2962–2827 cm^{-1}. This was shifted to ν_s (O–H) at 3421 cm^{-1}, and the ν_{as} (O–H) was found at 3066 cm^{-1} in the CP. A shift in the ν_{as} (C = O) of the ligand from 1685 cm^{-1} to ν_s (C = O) 1665 cm^{-1} in the CPs was observed While the ν_{as} (C = C) was shifted to 1558 cm^{-1} on the CPs, and the (M–O) band was seen around 443 cm^{-1} which suggests the coordination of the ligand to the metal, confirming the formation of new product $[Co(TPA)_2(H_2O)_2]$.

5.6 UV–visible spectra analysis of CPs

The data obtained from the UV–Visible spectra of the ligand and the CPs, presented below, indicates that there was strong absorption in the UV region of the electromagnetic spectrum, which is due to absorption by the ligands and also absorption was recorded at the visible region of the electromagnetic spectrum, which indicates that there were metal d-d transitions and hence the CPs should be colorloured.

(NB: Zn-MOF = $[Zn(TPA)_2(H_2O)_2]$, Co-MOF = $[Co(TPA)_2(H_2O)_2]$, and Ni-MOF = $[Ni(TPA)_2(H_2O)_2]$).

The electronic absorption spectra of the CPs, as shown in Fig. 8, were different from that of the synthesised terephthalic acid, specifically for the coloured compounds. It can

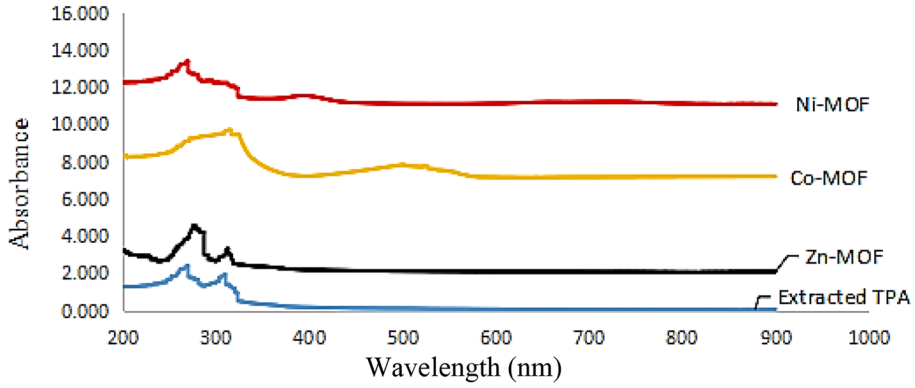


Fig. 8 Result showing UV–Vis Spectra of the CPs

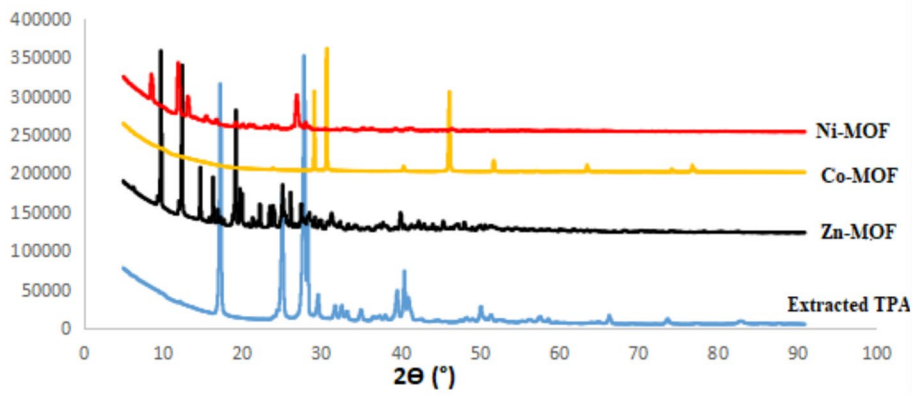


Fig. 9 PXRD pattern of the Synthesised Coordination Polymers from TPA

be seen that terephthalic acid showed bands at 262 nm, π→π* which was assigned and 309 nm, which was assigned π→π*. The above information shows that the ligand will be colourless.

The $[Ni(TPA)_2(H_2O)_2]$ showed six absorptions at 269, 308, 350, 419, 657, 734, which were attributed to $\pi \rightarrow \pi^*, n \rightarrow \delta^*, n \rightarrow \pi^*, 3A_{2g} \rightarrow 3T_{1g}(P), 3A_{2g} \rightarrow 3T_{1g}, 3A_{2g} \rightarrow 3T_{2g}$ respectively, which was as a result of ligand and d-d transitions.

The $[Zn(TPA)_2(H_2O)_2]$showed three absorptions at 279, 314 and 358, which were assigned $\pi \rightarrow \pi^*, n \rightarrow \delta^* and\ n \rightarrow \pi^*$respectively. The CP has a d^{10} electronic configuration, and does not absorb in the visible region and does not have a d-d transition. All these compounds absorbed in the UV regions are expected to be colourless.

The $[Co(TPA)_2(H_2O)_2]$ showed six absorptions at 280, 316, 350, 507, 652 and 771, which were assigned $\pi \rightarrow \pi^*, n \rightarrow \delta^*, n \rightarrow \pi^*, 3T_{1g} \rightarrow 3T_{1g}(P), 3T_{1g} \rightarrow 3A_{2g}\ and\ 3T_{1g} \rightarrow 3T_{2g}$ respectively, as a result of electronic and d-d transitions.

5.7 PXRD analysis result of the CPs

The PXRD patterns of individual CPs are presented in Fig. 9. The pattern of the PXRD of all the CPs showed characteristic peaks that are different from those of terephthalic

Table 5 BET surface area (m^2/g) and Langmuir surface area (m^2/g) results

Sample	BET surface area (m^2/g)	Langmuir surface area (m^2/g)
$[Ni(TPA)_2(H_2O)_2]$	347.830	87.67
$[Co(TPA)_2(H_2O)_2]$	348.908	84.73
$[Zn(TPA)_2(H_2O)_2]$	357.350	87.11

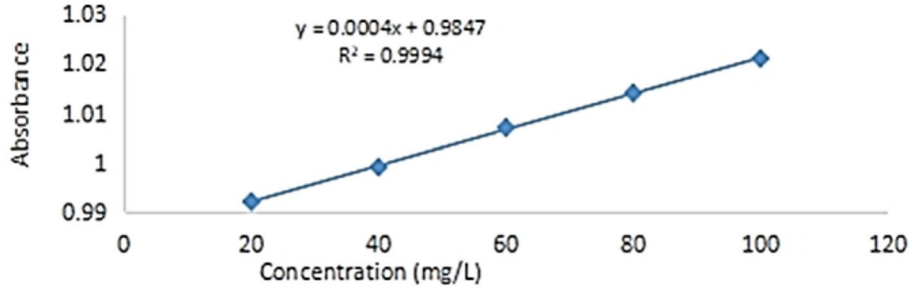


Fig. 10 Calibration curve showing the plot of absorbance against initial concentrations (Co) of Atrazine

acid. $[Zn(TPA)_2(H_2O)_2]$ showed characteristic peaks at 2θ values of 9.79°, 12.47°, 14.67 °, 16.47 °, 19.26 ° and 26.44 °, which are different from terephthalic acid peaks.

$[Ni(TPA)_2(H_2O)_2]$ also showed characteristic peaks which are different from terephthalic acid at 2θ values of 8.66°, 12.18°, 13.37 ° and 27.04 °. The PXRD obtained from $[Co(TPA)_2(H_2O)_2]$ showed characteristic peaks at 2θ values of 29.03°, 29.13°, 45.98° and 52.76 °, which are also different from terephthalic acid peaks at 2θ. When these data were compared to the Cambridge Crystallographic Data Centre (CCDC), powder diffraction pattern of the complexes that obtained from the mechanochemical method is identical to that of $Zn_3(OH)_4(C_8H_4O_4)$ complex, with CCDC no. 295966 previously reported by [8] and $[Ni_3(OH)_2(C_8H_4O_4)_2(H_2O)_4].2H_2O$ complex, with CCDC no. 638866, previously reported by Finisia et al. [13], although different synthetic condition was used.

(NB: Zn-MOF = $[Zn(TPA)_2(H_2O)_2]$, Co-MOF = $[Co(TPA)_2(H_2O)_2]$, and Ni-MOF = $[Ni(TPA)_2(H_2O)_2]$).

5.8 BET analysis results

Isotherms of N_2 adsorption/desorption of the powder samples of single and bimetal CPs, measurements of the pore volume, Langmuir surface area and surface area of the sample were carried out by BET analysis. The BET surface area values are shown in Table 5.

It can be deduced from the result that $[Zn(TPA)_2(H_2O)_2]$ has the highest BET surface area (m^2/g) of 357.350 (m^2/g), these was closely followed by $[Co(TPA)_2(H_2O)_2]$ and $[Ni(TPA)_2(H_2O)_2]$with BET surface area of 348.908 (m^2/g) and 347.830 (m^2/g) respectively.

6 Results of adsorption experiments

6.1 Calibration of atrazine

The stock solution (1000 mg/L) of Atrazine was used to prepare 20 mg/L, 40 mg/L, 60 mg/L, 80 mg/L, and 100 mg/L by diluting 2 ml, 4 ml, 6 ml, 8 ml and 10 ml of Atrazine stock solution with 100 ml of water respectively. The absorbance of the solution was taken using UV–Vis at a wavelength of 223 nm [2]. The result of the calibration showed a linearity, for which the R^2 value for Atrazine was found to be 0.999 (Fig. 10).

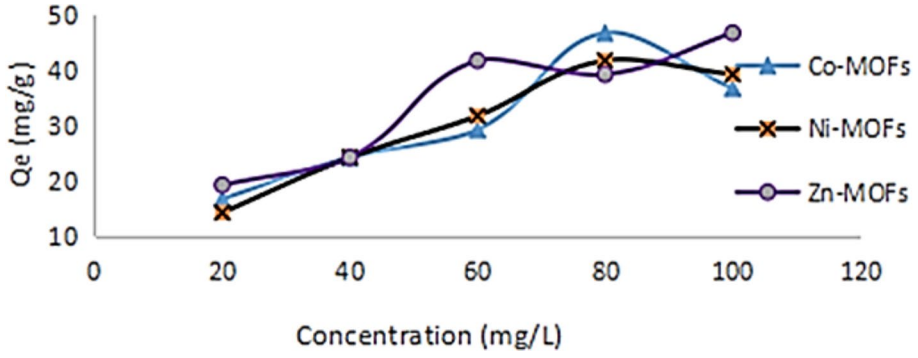


Fig. 11 Effect of concentration on the quantity of Atrazine adsorbed

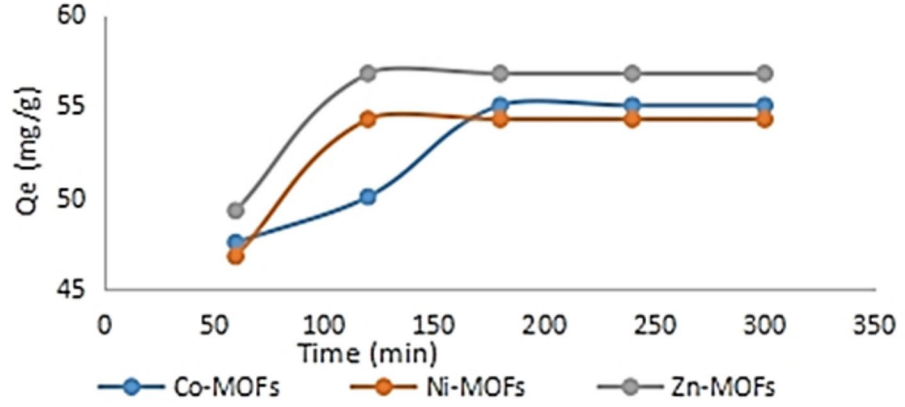


Fig. 12 Effect of time on quantity of Atrazine adsorbed

6.2 Effect of initial concentration

The values of Q_e were calculated using Eq. 1, and a curve was obtained by plotting Q_e against the initial concentration of adsorbate (Fig. 11), which shows the effect of concentration on the adsorption of Atrazine from solution. The effect of the concentration of Atrazine on the adsorption process was determined. The results from the graph (Fig. 11) show that $[Co(TPA)_2(H_2O)_2]$, $[Ni(TPA)_2(H_2O)_2]$ and $[Zn(TPA)_2(H_2O)_2]$ have optimized concentrations of 80, 80 and 100 mg/L, respectively, for Atrazine adsorption [2]. (0.01 g of the $[Co(TPA)_2(H_2O)_2]$, $[Ni(TPA)_2(H_2O)_2]$ and $[Zn(TPA)_2(H_2O)_2]$ at various Concentration of 20–100 mg/L, temperature of 28±2 C, pH of 7.0, and shaked at 100 rpm for 120 min).

6.3 Effect of time

The equilibrium time for the adsorption of Atrazine onto the different CPs at the optimised concentrations for the $[Co(TPA)_2(H_2O)_2]$, $[Ni(TPA)_2(H_2O)_2]$ and $[Zn(TPA)_2(H_2O)_2]$ adsorbents were studied. These concentrations were 80, 80 and 100 mg/L, respectively, for Atrazine. Using 0.01 g of the adsorbents and at a pH of 7.0, a temperature of 28±2 C with 100 rpm agitation speed for 120 min. The values of Qe were calculated at the $[Co(TPA)_2(H_2O)_2]$, $[Ni(TPA)_2(H_2O)_2]$ and $[Zn(TPA)_2(H_2O)_2]$ optimised time of 180, 120 and 120 min, respectively, for Atrazine (Fig. 12) (0.01 g of the $[Co(TPA)_2(H_2O)_2]$, $[Ni(TPA)_2(H_2O)_2]$and $[Zn(TPA)_2(H_2O)_2]$ at optimized

concentration, temperature of 28±2 C, pH of 7.0, and shaked at 100 rpm agitation speed for various time within the range of 60–300 min).

6.4 Effect of pH and results of point of zero charge

For the study of the effect of pH on the adsorption of Atrazine by the CPs, the optimized concentration of Atrazine for the $[Co(TPA)_2(H_2O)_2]$, $[Ni(TPA)_2(H_2O)_2]$ and $[Zn(TPA)_2(H_2O)_2]$ adsorbents utilized were 80, 80 and 100 mg/L at time of 180, 120 and 120 min respectively (Fig. 13a). Using 0.01 g of the adsorbents and varying pH within the range of 2–14 at a temperature of 28± 2 C and an agitation speed of 100 rpm, the values of Qe was calculated and the results (Fig. 13) shows that the CPs, $[Co(TPA)_2(H_2O)_2]$, $[Ni(TPA)_2(H_2O)_2]$ and $[Zn(TPA)_2(H_2O)_2]$, have optimum pH of Atrazine adsorption of 2, 4 and 2 respectively.

(by 0.01 g of the $[Co(TPA)_2(H_2O)_2]$, $[Ni(TPA)_2(H_2O)_2]$and $[Zn(TPA)_2(H_2O)_2]$ at optimized concentration, temperature of 28 ± 2 C, optimized time)

The results of the pH_{PZC} for the adsorbents are presented in Fig. 13b. The results indicated that the pH_{PZC} of $[Ni(TPA)_2(H_2O)_2]$ was found to be ≈ 6.3, whereas the pH_{PZC} of $[Co(TPA)_2(H_2O)_2]$ for this study was found to be ≈ 6.8, respectively. Also, the pH_{PZC} of $[Zn(TPA)_2(H_2O)_2]$ for this study was found to be ≈ 7.2 [17]. Each of the CPs has a positively charged surface below its pH_{PZC} (pH = 6.0), and in this medium, anions are probably adsorbed on the surface. On the other hand, adsorptions of cations are favoured above the pH_{PZC} of each of the CPs (pH = 8.0). This indicates that Atrazine are adsorbed below the pH_{PZC} of each of the CPs. This is due to weak electrostatic attraction between the positive surface of the adsorbent (CPs) and anions of Atrazine, which favours the accumulation of these pesticides on the surface of the adsorbent.

6.5 Effect of adsorbent dosage

In this study, the optimized concentration, time and pH for Atrazine adsorption by the $[Co(TPA)_2(H_2O)_2]$, $[Ni(TPA)_2(H_2O)_2]$ and $[Zn(TPA)_2(H_2O)_2]$ CPs were utilized. Using 0.01 g to 0.05 g of the adsorbents and at a temperature of 28±2 C with an agitation speed of 100 rpm, the values of Qe was calculated and the results (Fig. 14) shows that $[Co(TPA)_2(H_2O)_2]$, $[Ni(TPA)_2(H_2O)_2]$ and $[Zn(TPA)_2(H_2O)_2]$ have optimum dose of 0.03 g, 0.03 g and 0.02 g respectively for the adsorption of Atrazine. (between 0.01 g to 0.05 g of the $[Co(TPA)_2(H_2O)_2]$, $[Ni(TPA)_2(H_2O)_2]$and $[Zn(TPA)_2(H_2O)_2]$at optimized

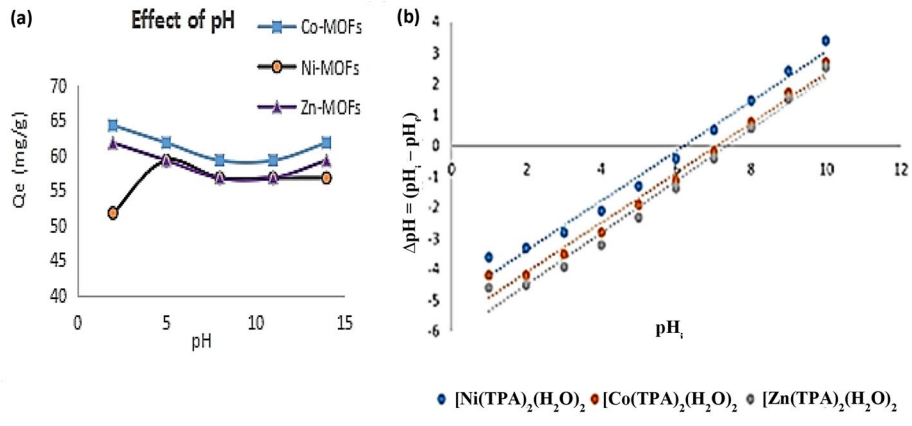


Fig. 13 **a** Effect of pH on the quantity of Atrazine adsorbed; **b** pHPZC for the adsorbents

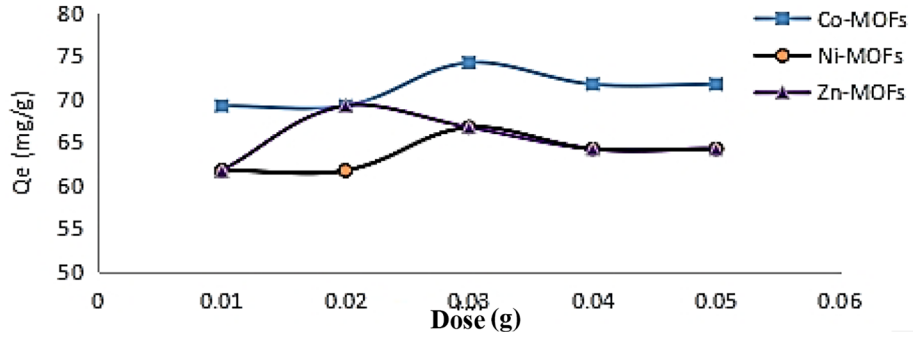


Fig. 14 Effect of adsorbent dose on the quantity of Atrazine adsorbed

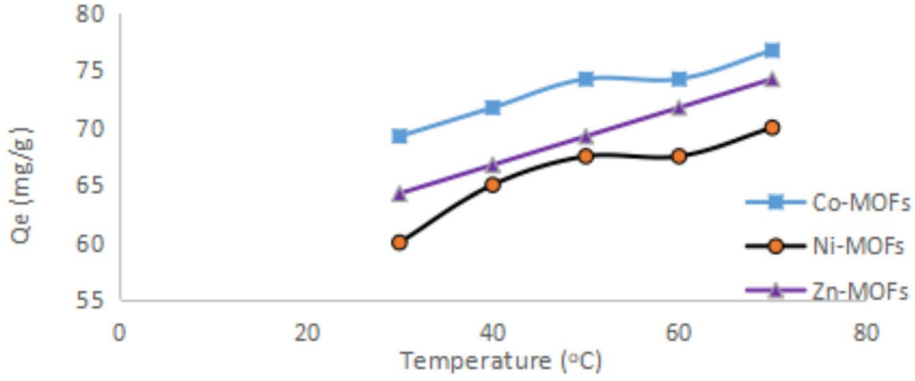


Fig. 15 Effect of temperature on the quantity of Atrazine adsorbed

concentration, temperature of 28±2 C, optimized time, shaked at 100 rpm agitation speed at optimized pH).

6.6 Effect of temperature

In this study, the optimum time, pH, adsorbent dose, and concentration for Atrazine adsorption by the $[Co(TPA)_2(H_2O)_2]$, $[Ni(TPA)_2(H_2O)_2]$ and $[Zn(TPA)_2(H_2O)_2]$ adsorbents were utilized at a temperature range of 30 C to 70 C with an agitation speed of 100 rpm. The values of Qe was calculated and $[Co(TPA)_2(H_2O)_2]$, $[Ni(TPA)_2(H_2O)_2]$ and $[Zn(TPA)_2(H_2O)_2]$ showed optimized temperature at 70 °C each for Atrazine (Fig. 15).

Between optimized adsorbent doses of $[Co(TPA)_2(H_2O)_2]$, $[Ni(TPA)_2(H_2O)_2]$and $[Zn(TPA)_2(H_2O)_2]$ at optimized concentration, optimized time, shaken at 100 rpm agitation speed at optimized pH.

6.7 Adsorption efficiency of adsorbents

The efficiency studies were carried out on individual adsorbents for Atrazine at optimum concentration for each of the adsorbents, temperature of 30 C, pH of 7, at an agitation speed of 100 rpm for 60 min.

The result (Fig. 16) shows that the removal of Atrazine has removal efficiency of 58.4% on $[Co(TPA)_2(H_2O)_2]$ while $[Ni(TPA)_2(H_2O)_2]$was closely followed with removal efficiency of 52.2% and was closely followed by $[Zn(TPA)_2(H_2O)_2]$with efficiency removal of 46.8%0.6.8 Adsorption Isotherms Study.

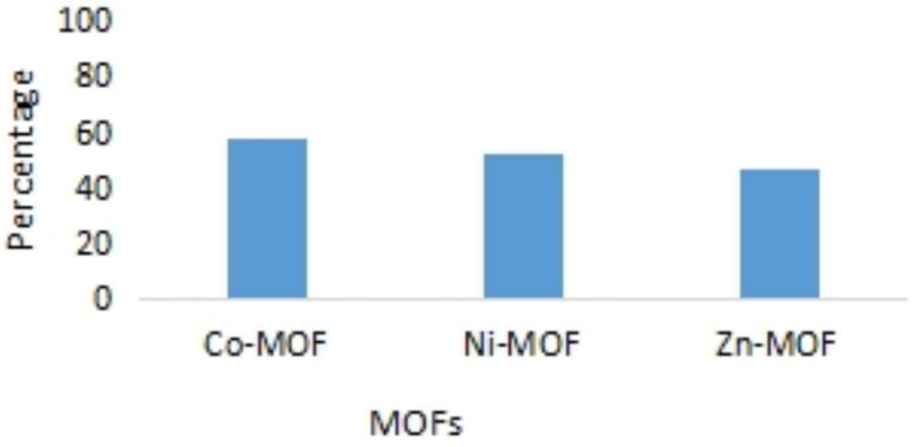


Fig. 16 % Removals of Atrazine using different adsorbents

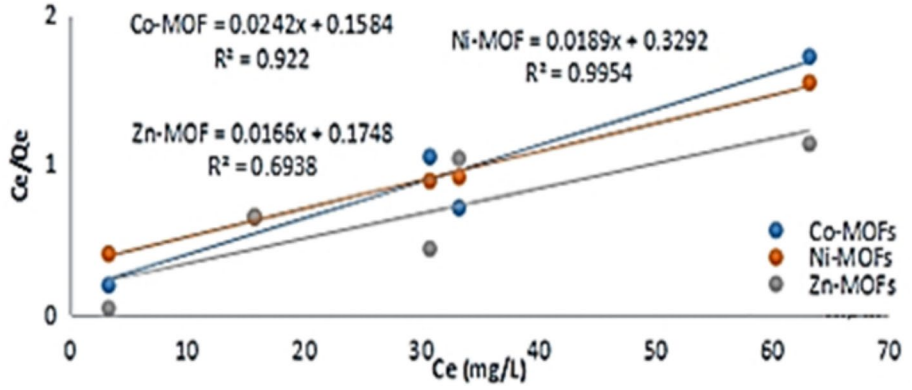


Fig. 17 Langmuir Isotherm plot for the adsorption of Atrazine

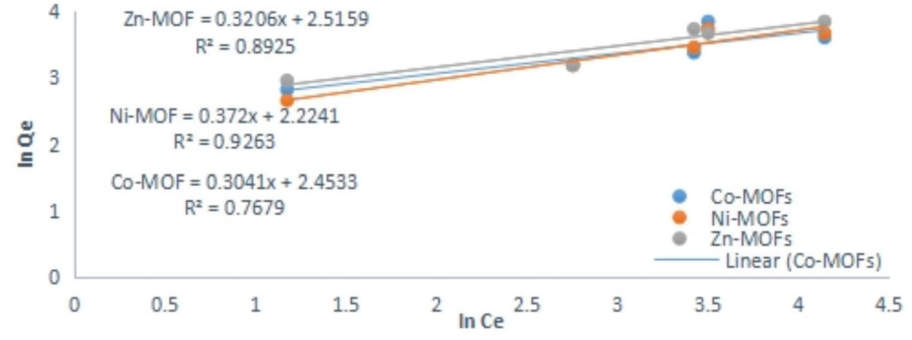


Fig. 18 Freundlich Isotherm plot for the adsorption of Atrazine

6.8 Adsorption isotherms study

An adsorption isotherm is a crucial description of the interaction between adsorbents and solutes. Many models have been made known over the years for testing the equilibrium for the adsorption of substances from their solution. The adsorption data obtained from this work were tested with Langmuir and Freundlich adsorption isotherms (Figs. 17 and 18). Table 6 represents the comparison of the R^2 values obtained for the adsorption process [4].

Table 6 Calculated equilibrium constants (K_L, K_F, q_m, n and correlation coefficient (R^2) for the adsorption of Atrazine on various CPs

	Langmuir Isotherm			Freundlich Isotherm		
CPs	**Q_m (mg/g)**	**K_L(L/mg)**	**R^2**	**K_F (mg/g)(L/g)$^{1/n}$**	**n**	**R^2**
$[Co(TPA)_2(H_2O)_2]$	41.32	0.15	0.92	12.38	0.73	0.77
$[Ni(TPA)_2(H_2O)_2]$	52.91	0.057	0.99	9.25	0.69	0.93
$[Zn(TPA)_2(H_2O)_2]$	60.24	0.095	0.69	11.27	0.74	0.89

The Langmuir model is mathematically represented as;

$$\frac{Ce}{q_e} = \frac{1}{q_m kl} + \frac{Ce}{q_m} \tag{2}$$

where q_m is the maximum sorption capacity (mg/g), k_l is the Langmuir constant, qe is the amount of adsorbate per unit mass of adsorbent (mg/g), and C_e is the equilibrium concentration of the adsorbate (mg/l).

It describes the sorption capacity and the correlation coefficient (R^2) value of 0.92, 0.99 and 0.69 respectively $[Co(TPA)_2(H_2O)_2]$, $[Ni(TPA)_2(H_2O)_2]$ and $[Zn(TPA)_2(H_2O)_2]$ on Atrazine. The maximum sorption capacity q_m and mono-molecular layer K_L are found to be 41.322 mg/g and 0.153 L/g for $[Co(TPA)_2(H_2O)_2]$, 52.910 mg/g and 0.0574 L/g for $[Ni(TPA)_2(H_2O)_2]$ and 60.241 mg/g and 0.095 L/g for $[Zn(TPA)_2(H_2O)_2]$ on Atrazine.

For the Freundlich isotherm, the equation is given by;

$$\ln Qe = \ln K_F + \frac{1}{n} \ln Ce \tag{3}$$

where Q_e is the amount adsorbed at equilibrium per gram of the adsorbent (mg/g), K_f and n are the Freundlich constant, and C_e is the equilibrium concentration of the adsorbate (mg/l).

The plot of Inq_e vs In C_e gave straight line K_F for adsorption of Atrazine was found experimentally to be (12.38, 9.245 and 11.267 mg/g) respectively with n value of (0.73, 0.69 and 0.74) respectively and R^2 value of 0.89, 0.93, and 0.77 over $[Zn(TPA)_2(H_2O)_2]$, $[Ni(TPA)_2(H_2O)_2]$ and $[Co(TPA)_2(H_2O)_2]$. (over $[Co(TPA)_2(H_2O)_2]$, $[Ni(TPA)_2(H_2O)_2]$ and $[Zn(TPA)_2(H_2O)_2]$ at 298 K for 2 h at optimised pH). (over $[Co(TPA)_2(H_2O)_2]$, $[Ni(TPA)_2(H_2O)_2]$ and $[Zn(TPA)_2(H_2O)_2]$ at 298 K for 2 h at optimised pH).

In a bid to gain insight into the adsorption behavior of the various CPs ($[Co(TPA)_2(H_2O)_2]$, $[Ni(TPA)_2(H_2O)_2]$, and $[Zn(TPA)_2(H_2O)_2]$), the Langmuir and Freundlich isotherm models were applied to the adsorption data (Table 6). The Langmuir isotherm assumes monolayer adsorption onto a homogeneous surface, allowing determination of maximum adsorption capacity (Qm) and adsorption affinity (KL). Among the three CPs, $[Zn(TPA)_2(H_2O)_2]$ demonstrated the highest Qm (60.24 mg/g), followed by $[Ni(TPA)_2(H_2O)_2]$ (52.91 mg/g) and $[Co(TPA)_2(H_2O)_2]$ (41.32 mg/g). This trend reflects the influence of the metal centre on adsorption capacity, consistent with findings from previous studies where Zn-based materials exhibited enhanced adsorption due to their higher surface activity [18]. Although $[Zn(TPA)_2(H_2O)_2]$ showed the highest capacity, its R2 = 0.69 for the Langmuir isotherm was the lowest, indicative of a deviation from ideal monolayer adsorption and a possible heterogeneous surface. Conversely, $[Ni(TPA)_2(H_2O)_2]$ had a strong R2 of 0.99, where monolayer adsorption is presumed to predominate in the process. We note that $[Co(TPA)_2(H_2O)_2]$ exhibited a K_L value of 0. 15 L/mg, possibly indicating greater initial binding affinity to the adsorbate, a fact that

has been reported previously by Ali et al. (2021) for cobalt-based frameworks containing polar functional groups to facilitate affinity binding to the adsorbate.

The Freundlich isotherm, which accounts for adsorption on heterogeneous surfaces, provided additional insights. The Freundlich constant K_F was highest for $[Co(TPA)_2(H_2O)_2]$ (12.38), but the adsorption intensity (n) was most favourable for $[Ni(TPA)_2(H_2O)_2]$ (n = 0.93), indicating relatively uniform adsorption across different concentration ranges. These results align with previous reports showing that Ni-based CPs often demonstrate more favourable adsorption kinetics and thermodynamics due to their moderate electronegativity and stability [20]. The R2 values further supported the Freundlich model's applicability to $[Ni(TPA)_2(H_2O)_2]$ (R2 = 0.93) and $[Zn(TPA)_2(H_2O)_2]$ (R2 = 0.89), whereas $[Co(TPA)_2(H_2O)_2]$ showed a poorer fit (R2 = 0.77).

6.9 Adsorption kinetics

The kinetic study is very important in the adsorption study, which gives an idea about the rate of adsorbate uptake and the efficiency of adsorption. The mechanism of adsorption depends on the physical and chemical properties of the adsorbent as well as the mass transfer process. It provides an understanding of the adsorption rate and the controlling mechanism of the process [29].

For Pseudo-first order, the adsorption data were examined with the pseudo-first-order kinetic model, which is represented by the equation:

$$\ln (q_e - qt) = \ln q_m - k_1 t \tag{4}$$

A plot of ln (qe – qt) against time (t) was obtained, and the values of the first-order kinetic constant (k_1) were determined by K_1 = – slope.

For Pseudo-second order, the adsorption data were tested by the equation:

$$\frac{t}{q_t} = \frac{1}{k_2 q^2 e} + \frac{t}{q_e} \tag{5}$$

A plot of t/q_t against time was obtained, and the values of the second-order kinetic constant (k_1) were determined by.

where R^2 is the correlation coefficient, q_e (exp) is the experimentally measured adsorbate concentration at equilibrium, q_e (cal) is the calculated adsorbate concentration at equilibrium, and K_2 is the rate constant of pseudo-second order adsorption. The regression coefficient values (R^2) showed the appropriateness of the kinetic model to the adsorption process (Figs. 19 and 20). The values obtained show that the pseudo-first order kinetic model is suitable for the adsorption process studied, as shown in Table 7 and Figs. 19 and 20. This result indicates that the adsorption process is more of physisorption in nature for the three adsorbents studied [29]. (over $[Co(TPA)_2(H_2O)_2]$, $[Ni(TPA)_2(H_2O)_2]$ and $[Zn(TPA)_2(H_2O)_2]$ at 298 K at optimised pH).

6.10 Adsorption thermodynamics

Temperature has an impact on the adsorption capacity to an extent. It is well known that a temperature change alters the adsorption equilibrium in a specific way determined by the exothermic or endothermic nature of a process. In the study, the effect of temperature (Fig. 21 and Table 8) was studied in the range 303 to 343 K to determine the

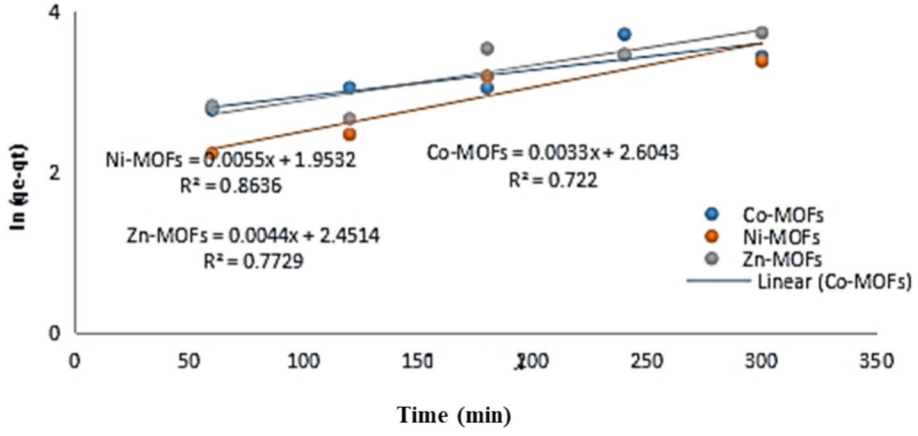


Fig. 19 Pseudo-First Order Kinetics Isotherm plot for the adsorption of Atrazine

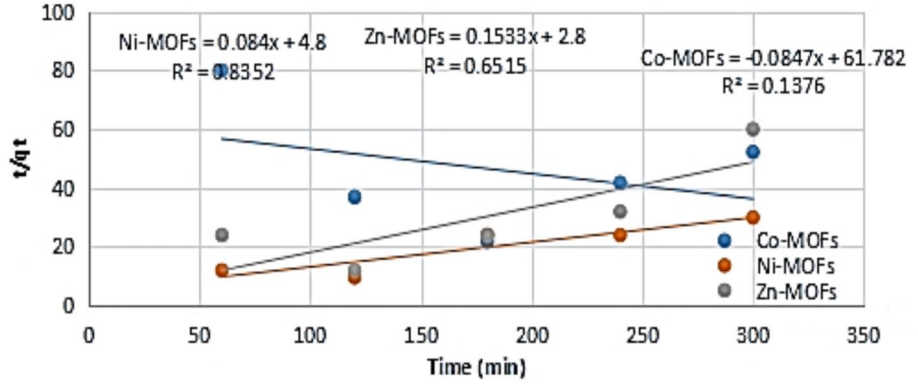


Fig. 20 Pseudo-second order Kinetics Isotherm plot for the adsorption of Atrazine

Table 7 Pseudo-First Order and Pseudo-Second Order Kinetics plot for the adsorption of Atrazine over $[Co(TPA)_2(H_2O)_2]$, $[Ni(TPA)_2(H_2O)_2]$ and $[Zn(TPA)_2(H_2O)_2]$ at 298 K at optimised pH

	Pseudo-First Order			Pseudo-Second Order		
Adsorbent	**$K_1(min^{-1})$**	**q_e (mg/g)**	**R^2**	**$K_2(gmin^{-1}/mg)$**	**q_e (mg/g)**	**R^2**
$[Zn(TPA)_2(H_2O)_2]$	0.0033	13.62	0.72	− 0.085	− 11.81	0.14
$[Co(TPA)_2(H_2O)_2]$	0.0055	7.05	0.86	0.084	11.91	0.84
$[Ni(TPA)_2(H_2O)_2]$	0.0044	11.6	0.77	0.15	6.52	0.65

thermodynamic feasibility of the adsorption process of Atrazine solutions on respective CPs (Kumar et al., 2014).

The equation is given by;

$$\ln K_l = \frac{\Delta S_0}{R} - \frac{\Delta H_0}{RT} \tag{6}$$

where K_l is the ratio of Qe/Ce, ΔS° is the entropy change (J/molK^{-1}), and ΔH° is the enthalpy change (KJ/mol). (over $[Zn(TPA)_2(H_2O)_2]$, $[Cu(TPA)_2(H_2O)_2]$ and $[Ni(TPA)_2(H_2O)_2]$ between 303 and 343 K for 2 h at optimised pH).

The values of ΔH° for Atrazine are all positive, indicating the endothermic nature of the process, which further explains the fact that the adsorption efficiency increased with the increase of temperature. The magnitude of ΔH° may also give an idea about the type

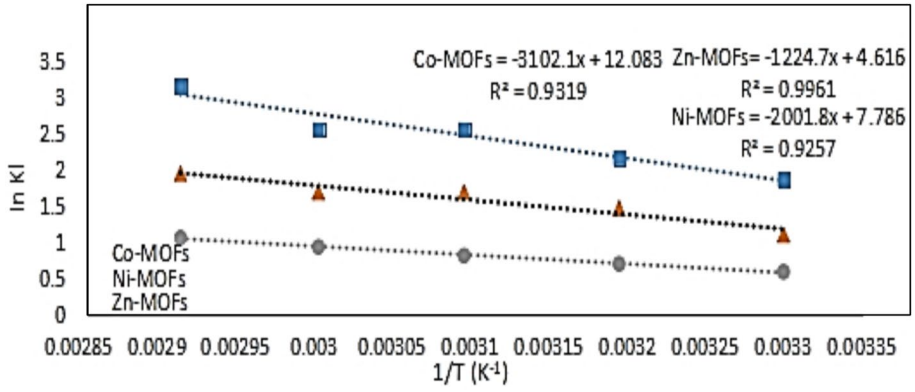


Fig. 21 Thermodynamics plot for the adsorption of Atrazine

Table 8 Thermodynamic parameters on the adsorption of Atrazine on Various CPs

Adsorbent	ΔH° (KJ/mol)	ΔS° (J/mol/K)	ΔG° (J/mol) at different temperatures				
			303 K	313 K	323 K	333 K	343 K
$[Co(TPA)_2(H_2O)_2]$	25.79	100.46	− 4692.7	− 5628.67	− 6869.95	− 7082.64	− 9016.79
$[Ni(TPA)_2(H_2O)_2]$	16.64	64.733	− 2767.56	− 3815.82	− 4528.69	− 4668.9	− 5549.16
$[Zn(TPA)_2(H_2O)_2]$	10.18	38.377	-1476.6	− 1813.53	− 2180.11	− 2580.56	− 3019.96

Table 9 Performance evaluation of $[Zn(TPA)_2(H_2O)_2]$ on Atrazine removal

Adsorbent	Q_m (mg/g)	References
$[Zn(TPA)_2(H_2O)_2]$	60.24	This work
Magnetic porous carbon	21.0	[9]
NU-1000-(Zr)	36.0	[2]
RWAC-1 Raw waste	13.95	[16]
JPC Jackfruit peel	20.12	[21]
BC-800 Sawdust	48.6	[15]
BC-850 Corn stalk	40.60	[36]

of sorption. The ΔH° values were found to be between + 9.81 and + 27.73 kJ/mol for Atrazine, and this indicates that physisorption is the major adsorption mechanism [4].

6.11 Comparison study

The uptake of Atrazine by ($[Zn(TPA)_2(H_2O)_2]$) was compared with other adsorbents previously reported in literature for the removal of Atrazine from an aqueous medium (Table 9). It was observed that the uptake was higher than adsorbents used by other researchers, such as Chen et al. [9], Jain et al. [21] and Tao et al. [36] at experimental conditions of 2 h contact time, initial atrazine concentration of 100 mg/L, and adsorbent dosage of 0.01 g for this study.

6.12 Adsorption mechanisms

The possible mechanism of high adsorption capacity (Fig. 22) and fast adsorption rate of Atrazine on ($[Zn(TPA)_2(H_2O)_2]$, $[Cu(TPA)_2(H_2O)_2]$ and $[Ni(TPA)_2(H_2O)_2]$) can be explained by hydrogen bonding, 𝜋−𝜋 interaction, electrostatic interaction and Van der Waals forces between them [23]. The hydrogen bonding and electrostatic interaction can occur between $[Zn(TPA)_2(H_2O)_2]$, $[Cu(TPA)_2(H_2O)_2]$ and $[Ni(TPA)_2(H_2O)_2]$ surface

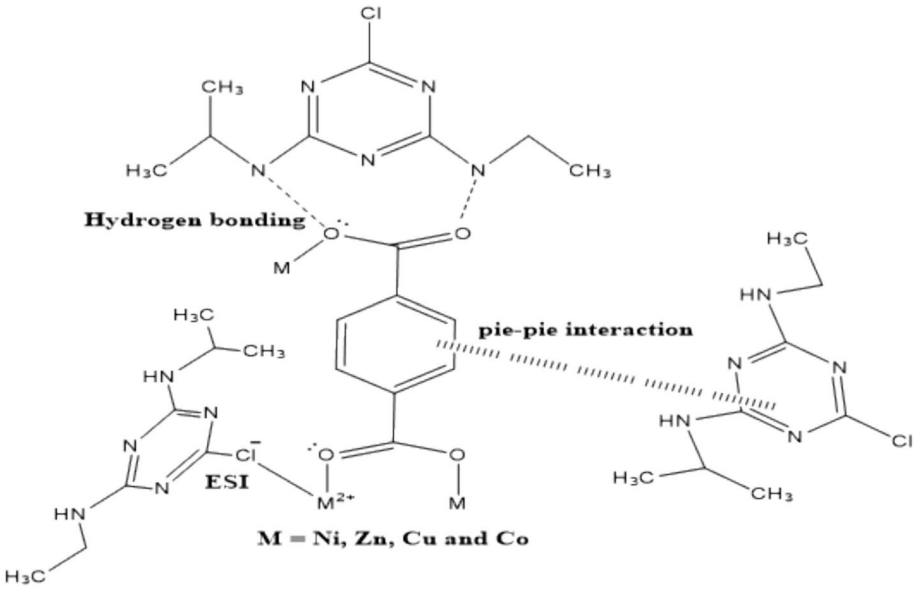


Fig. 22 Mechanism of atrazine adsorption with the adsorbent

with the lone-pair of nitrogen in atrazine. The CPs, therefore, exhibit positive surface excess through the central metals while the adsorbate exhibits negative surface excess for electrostatic interactions. Also, the Van der Waals forces arise because of temporary distortions of the electron orbital surrounding the CPs and the Atrazine.

7 Conclusion

Terephthalic acid was successfully extracted from plastic bottle waste. Some 3d metal–organic frameworks (Ni^{2+}, Zn^{2+}, and Co^{2+}) using terephthalate ligand extracted from plastic waste were successfully prepared by the mechanochemical method via ball-milling. The CPs were used for the removal of Atrazine pesticide (an endocrine-disrupting chemical) from aqueous solution.

The batch experiments were carried out to understand its applicability in the removal of Atrazine pesticide from a polluted environment. The results show $[Co(TPA)_2(H_2O)_2]$, $[Ni(TPA)_2(H_2O)_2]$, and $[Zn(TPA)_2(H_2O)_2]$ have maximum adsorption capacities of 41.32, 52.91 and 60.24 mg/g, respectively, on Atrazine. The high adsorption of $[Zn(TPA)_2(H_2O)_2]$ as compared to others may be suggested to be attributed to its high porosity, smaller particle sizes and high crystalline nature. The kinetics studies showed that the adsorption of Atrazine followed a pseudo-first-order model. Our results revealed that $[Co(TPA)_2(H_2O)_2]$, $[Ni(TPA)_2(H_2O)_2]$ and $[Zn(TPA)_2(H_2O)_2]$ could be used as effective adsorbents for the removal of Altrazine pesticide from wastewater.

This research work presents a novel approach to the extraction of value-added chemicals from plastic wastes and environmental remediation (plastic pollution minimisation) by creating an efficient adsorbent (MOFs) for atrazine removal. This innovative strategy combines sustainability with practical applications in water treatment, showcasing the potential of circular economy principles in addressing environmental challenges.

Abbreviations

TPA	Terephthalic acid/Benzene-1,4-dicarboxylic acid
Co-MOF	$[Co(TPA)_2(H_2O)_2]$
Zn-MOF	$[Zn(TPA)_2(H_2O)_2]$

Ni-MOF $[Ni(TPA)_2(H_2O)_2]$
CPs Coordination polymers

Authors contributions
AC Tella : Conceptualization, Methodology, Data curation, Writing –original draft. **UV Ugwuanyi:** Conceptualization, Methodology, Data curation, Writing –original draft. **VT Olayemi:** Conceptualization, Methodology, Data curation, Writing –original draft. **OG Adeyemi:** Formal analysis, Supervision, Writing –review & editing, Methodology, Supervision, Writing –review & editing. **HS Clayton:** Formal analysis, Supervision, Writing –review & editing, Formal analysis, Investigation **DP Fapojuwo:** Formal analysis, Investigation, Review&editing **MD Olawale**: Formal analysis, DFT and Computational studie, Review & editing **VO Adimula:** Formal analysis, Writing –review & editing, Methodology, Supervision, Writing –review & editing. **SO Owalude:** Formal analysis, Supervision, Funding acquisition, Writing –review & editing, Methodology, Supervision, Writing –review & editing.

Funding
The work was funded by the research grant awarded by Organization for the Prohibition of Chemical Weapons(OPCW) (L/ICA/ICB-327/23).

Data availability
All data generated or analysed during this study are included in the manuscript.

Declarations

Ethics approval and consent to participate
Not applicable

Consent for publication
Not applicable.

Competing interests
The authors declare no competing interests.

Author details
[1]Department of Chemistry, University of Ilorin, P.M.B 1515, Ilorin, Nigeria
[2]Department of Chemistry, Kwara State University, Malete, Nigeria
[3]Department of Chemical Sciences, Redeemer's University, Ede, Nigeria
[4]Department of Chemistry, University of South Africa, Pretoria, South Africa
[5]Department of Chemistry, Nelson Mandela Metropolitan University, Port Elizabeth, South Africa
[6]Department of Physical and Chemical Sciences, Elizade University, Ilara Mokin, Nigeria
[7]Department of Industrial Chemistry, University of Ilorin, P.M.B 1515, Ilorin, Nigeria
[8]Department of Advanced Material Science, National University of Science and Technology MISIS, Moscow, Russia

Received: 17 December 2024 / Accepted: 1 December 2025
Published online: 10 December 2025

References

1. Ahmed SHJ. Composites of metal-organic frameworks: Preparation and application in adsorption. Mater Today. 2014;17(2014):136–46.
2. Akpinar IAO. Adsorption of atrazine from water in metal-organic framework materials. J Chem Eng Data. 2018;63(2018):2368–75.
3. Ali I, Asim M, Khan TA. Low cost adsorbents for the removal of organic pollutants from wastewater. J Environ Manage. 2012;113(2018):170–83.
4. Ayawei N, Horsfall Jnr M, Spiff I. *Rhizophora mangle* waste as adsorbent for metal ions removal from aqueous solution,. Eur J Sci Res. 2017;9(1):21.
5. Bamigbose JT, Elaigwu SE, Adimula VO, Okeowo HO, Olayemi VT, Ameen OA, et al. Green route synthesis and adsorption of copper –benzimidazole coordination polymer for removal of methyl orange from water. Chem Afr. 2023;6(5):2581–92.
6. Bernini MC, Sapag K. Polyethylene terephthalate (PET) waste and its test in CO_2 adsorption synthesis of MOF-5 using terephthalic acid as a ligand obtained from polyethylene terephthalate (PET) waste and its test in CO_2 adsorption. Br J Chem Eng. 2022. https://doi.org/10.1007/s43153-021-00192-5.
7. Bai YH, Zhou L, Wang J. Organo-phosphorous pesticides residues in market foods in Shaanxi area. Food Chem. 2006;98:240–2.
8. Carton A, Abdelouhab S, Renaudin G, Rabu P, François M. Structure of zinc hydroxy-terephthalate: $Zn_3(OH)_4(C_8H_4O_4)$. Solid State Sci. 2006;8(8):958–63. https://doi.org/10.1016/j.solidstatesciences.2006.02.043.
9. Chen D, Chen C, Shen W, Quan H, Chen S, Xie S, et al. MOF-derived magnetic porous carbon-based sorbent: Synthesis, characterization, and adsorption behavior of organic micropollutants. Adv Powder Technol. 2017;28(2017):1769–79.
10. Cook TR, Zheng YR, Stang PJ. Metal-organic frameworks and self-assembled supramolecular coordination complexes: comparing and contrasting the design, synthesis, and functionality of metal-organic materials. Chem Rev. 2013. https://doi.org/10.1021/cr3002824.
11. Deng H, Feng D, He J, Fang-ze L, Hua-mei Y, Cheng-jun G. Influence of biochar amendments to soil on the mobility of atrazine using sorption-desorption and soil thinlayer chromatography. Ecol Eng. 2017;99:381–90.

12. FAO (Food and Agricultural Organization) of the United Nations. Pesticides: Balancing Crop Protection and Responsible Use Plant Production and Protection Division. Rome: FAO; 2014.
13. Finisia Y, Tjahjanto RT, Prananto YP. Effect of solvent in the solvothermal synthesis of nickel(II)-terephthalate complex. Acta Chim Asiana. 2024;7(2):487–93. https://doi.org/10.29303/aca.v7i2.198.
14. Furukawa H, Cordova KE, O'Keeffe M, Yaghi OM. The chemistry and applications ofmetal-organic frameworks. Science. 2013;341:1230444. https://doi.org/10.1126/science.12304.
15. Gao Y, Jiang Z, Li J, Xie W, Jiang Q, Bi M, et al. A comparison of the characteristics and atrazine adsorption capacity of co-pyrolysed and mixed biochars generated from corn strawand sawdust. Environ Res. 2019;172:561–8. https://doi.org/10.1016/j.envres.2019.03.010.
16. Ghosh PK, Philip L. Performance evaluation of waste activated carbon on Atrazine removal from contaminated water. J Environ Sci Health B. 2005;40(3):425–41. https://doi.org/10.1081/pfc-200047576.
17. Giwa AA, Olajire AA, Oladipo MA, Bello MO, Bello IA. Adsorption of ternary metal system onto the sawdust of locust bean tree (*Parkia biglobosa*): equilibrium, kinetics and thermo- dynamics studies. Int J Sci Eng Res. 2013;4(6):1275–96.
18. Gupta VK, Kumar R, Nayak A, Saleh TA, Barakat MA. Adsorptive removal of dyes from aqueous solution onto carbon nanotubes: a review. Adv Coll Interface Sci. 2013;193(2013):24–34.
19. Hamilton DJ, Ambrus Á, Dieterle RM, Felsot AS, Harris CA, Holland PT, et al. Regulatory limits for pesticide residues in water (IUPAC technical report). Pure Appl Chem. 2003;75(8):1123–55. https://doi.org/10.1351/pac200375081123.
20. Hamza MF, Hamad NA, Hamad DM, Khalafalla MS, Abdel-Rahman AAH, Zeid IF, et al. Synthesis of eco-friendly biopolymer, alginate-chitosan composite to adsorb the heavy metals, Cd (II) and Pb (II) from contaminated effluents. Materials. 2021;14(9):2189.
21. Jain S, Yamgar R, Jayaram RV. Photolytic and photocatalytic degradation of atrazine in the presence of activated carbon. Chem Eng J. 2009;148(2–3):342–7. https://doi.org/10.1016/j.cej.2008.09.006.
22. Jonesa PG, Ossowski J, Kuś P, Dix I. Three crystal structures of terephthalic acid salts of simple amines. Zeitschrift Fur Naturforschung - Sect B J Chem Sci. 2009;64(7):865–70. https://doi.org/10.1515/znb-2009-0716.
23. Jung BK, Hasan Z. Adsorptive removal of 2,4-dichlorophenoxy- acetic acid (2,4-D) from water with a metal–organic framework. Chem Eng J. 2013;234(2013):99–105.
24. Kaduk JA. Conventional and eccentric uses of crystallographic databases in practical materials identification problems. J Res Natl Inst Stand Technol. 1996. https://doi.org/10.6028/jres.101.029.
25. Karayannidis GP, Chatziavgoustis AP, Achilias DS. Poly(ethylene terephthalate) recycling and recovery of pure terephthalic acid by alkaline hydrolysis. Adv Polym Technol. 2002;21(4):250–9. https://doi.org/10.1002/adv.10029.
26. Kumar M, Philip L. Adsorption and desorption characteristics of hydrophobic pesticide endosulfan in four Indian soils. Chemosphere. 2006;62:1064–77.
27. Li X. Metal-organic framework UIL-66 membranes. Front Chem Sci Eng. 2020;12:216–32.
28. Li JR, Sculley J, Zhou HC. Metal-organic frameworks for separations. Chem Rev. 2012;112:869–932.
29. Muthukumarana C, Sivakumar VM, Thirumarimurugan M. Adsorption isotherm and kinetic studies of crystal violet dye removal from aqueous solution using surfactant modified magnetic nano-adsorbent. J Taiwan Inst Chem Eng. 2016;63:354–62.
30. Naushadn M, Alothman ZA, Khan MR. Removal of malathion from aqueous solution using De-Acidite FF-IP resin and determination by UPLC–MS/MS: equilibrium, kinetics and thermodynamics studies. Talanta. 2013;115:15–23.
31. Ntoi, L. L. A., and Eschwege, K. G. Von. Spectrophotometry mole ratio and continuous variation experiments with dithizone.7 12 59–92.
32. Okoro HK, Tella AC, Ajibola OA, Zvinowanda C, Catherine Ngila J. Adsorptive removal of naphthalene and anthracene from aqueous solution with zinc and copper-terephthalate metal-organic frameworks. Bull Chem Soc Ethiop. 2019;33(2):229–41. https://doi.org/10.4314/bcse.v33i2.4.
33. Pesticides atlas-Nigeria. Heinrich-Böll-StiftungAbuja, Nigeria. 2022. https://ng.boell.org/en/pesticides-atlas-nigeria
34. Rojas S, Rodríguez-Diéguez A, Horcajada P. Metal-organic frameworks in agriculture. ACS Appl Mater Interf. 2022;14(15):16983–7007. https://doi.org/10.1021/acsami.2c00615.
35. Rowsell JL, Yaghi OM. Metal–organic frameworks: a new class of porous materials. Microporous Mesoporous Mater. 2004;73(1–2):3–14.
36. Tao Y, Han S, Zhang Q, Yang Y, Shi H, Akindolie MS. Application of biochar with functional microorganisms for enhanced Atrazine removal and Phosphorus utilization. J Clean Prod. 2020;257:120535. https://doi.org/10.1016/j.jclepro.2020.120535.
37. Tella AC, Owalude SO, Olatunji SJ, Adimula VO, Elaigwu SE, Alimi LO, et al. Synthesis of zinc-carboxylate metal-organic frameworks for the removal of emerging drug contaminant (amodiaquine) from aqueous solution. J Environ Sci. 2018;64:264–75. https://doi.org/10.1016/j.jes.2017.06.015.
38. Tella AC, Owalude SO, Ojekanmi CA, Oluwafemi SO. Synthesis of copper iso-nicotinate metal-organic frameworks simply by mixing solid reactants and investigation of their adsorptive properties for the removal of the fluorescein dye. New J Chem. 2014;38:4494–500.
39. Wang X, Song X, Sun K, Cheng L, Ma W. MOFs derived porous nanomaterials for gas sensing. Polyhedron. 2016;12:155–63.
40. WHO, 2003. International Statistical Classification of Disease & Related Health Problems, 10th revision, Toxic effects of pesticides, T60; Sequelae of toxic effects of substances chiefly nonmedical as source to:Ricketts, D.C. The Microbial Biodegradation of Paraquat in Soil. Pestic Sci. 2003;55(5):596–614.
41. Yaghi OM. Reticular synthesis and the design of new materials. Nature. 2005;423(6941):705.
42. Yingran H, Pantang Y, Dangchen M, Tai Shung CH. UiO-66 incorporated thin film nano composite membranes for efficient selenium and arsenic removal. Sci Total Environ. 2017;2022(838):156012.

Publisher's Note

Springer Nature remains neutral with regard to jurisdictional claims in published maps and institutional affiliations.